J Neurophysiol 104: 484–497, 2010.
First published May 12, 2010; doi:10.1152/jn.00297.2010.

Minor Contribution of Principal Excitatory Pathways to Hippocampal LFPs in the Anesthetized Rat: A Combined Independent Component and Current Source Density Study

A. Korovaichuk,[1,*] J. Makarova,[1,*] V. A. Makarov,[2,*] N. Benito,[1] and O. Herreras[1]

[1]*Department of Systems Neuroscience, Cajal Institute–Consejo Superior de Investigaciones Científicas, Madrid; and* [2]*Department of Applied Mathematics, Faculty of Mathematics, Universidad Complutense of Madrid, Madrid, Spain*

Submitted 26 March 2010; accepted in final form 6 May 2010

Korovaichuk A, Makarova J, Makarov VA, Benito N, Herreras O. Minor contribution of principal excitatory pathways to hippocampal LFPs in the anesthetized rat: A combined independent component and current source density study. *J Neurophysiol* 104: 484–497, 2010. First published May 12, 2010; doi:10.1152/jn.00297.2010. Analysis of local field potentials (LFPs) helps understand the function of the converging neuronal populations that produce the mixed synaptic activity in principal cells. Recently, using independent component analysis (ICA), we resolved ongoing hippocampal activity into several major contributions of stratified LFP-generators. Here, using pathway-specific LFP reconstruction, we isolated LFP-generators that describe the activity of Schaffer-CA1 and Perforant-Dentate excitatory inputs in the anesthetized rat. First, we applied ICA and current source density analysis to LFPs evoked by electrical subthreshold stimulation of the pathways. The results showed that pathway specific activity is selectively captured by individual components or LFP-generators. Each generator matches the known distribution of axonal terminal fields in the hippocampus and recovers the specific time course of their activation. Second, we use sparse weak electrical stimulation to prime ongoing LFPs with activity of a known origin. Decomposition of ongoing LFPs yields a few significant LFP-generators with distinct spatiotemporal characteristics for the Schaffer and Perforant inputs. Both pathways convey an irregular temporal pattern in bouts of population activity of varying amplitude. Importantly, the contribution of Schaffer and Perforant inputs to the power of raw LFPs in the hippocampus is minor (7 and 5%, respectively). The results support the hypothesis on a sparse population code used by excitatory populations in the entorhino-hippocampal system, and they validate the separation of LFP-generators as a powerful tool to explore the computational function of neuronal circuits in real time.

INTRODUCTION

Multiple neuronal populations form a complex system of local circuits and global networks whose activity constitutes the basis for information processing in the brain. The electrical transmembrane currents produced by working neurons are mixed together and generate local field potentials (LFPs), a macroscopic variable that reflects the information processing at mesoscopic scales. Thus the decoding of LFPs may help us understand the principles of information handling. To date, resolving the electrical activity of converging neuronal populations into the original informative sources remains problematic (Mitzdorf 1985; Nunez and Srinivasan 2006).

Approaches are emerging to analyze LFPs, such as spectral coherence, principal components, and laminar population analysis, and these have proven useful to identify important features in mixed deep electrical sources (for example, see Einevoll et al. 2007; Kocsis et al. 1999). Recently we implemented a blind source separation strategy (Makarov et al. 2010) that takes advantage of the spatial immobility of electrical brain sources in the LFP's time scale. This structural feature arises from the fixed location of the synaptic afferents to target cells, producing transmembrane currents whose extracellular part is circumscribed to the postsynaptic cell. The approach uses independent component analysis (ICA) to separate the informative sources (Bell and Sejnowski 1995; Makeig et al. 2004; Stone 2004), and it allowed us to disentangle intracerebral LFPs recorded in the hippocampal CA1 region into the contributions of a few major LFP-generators (Makarov et al. 2010). In this study, we present a special technique that permits the unequivocal association of the LFP-generators isolated with the presynaptic neuronal populations and its application to quantify the independent contribution of Schaffer and Perforant inputs to the total hippocampal LFP. Thus we have obtained a tool for the parallel readout of the discrete activities of the working neuronal populations from standard LFPs.

ICA is a widely used approach to extract spatially distinct independent sources of activity from mixed signals (for review, see Choi et al. 2005). Simultaneous multisite recordings are required to estimate the different impact of several spatially localized and distant generators into each sensor. This method has been successfully applied to surface EEG recordings, whereby deep strongly synchronized neural sources can be discriminated (Jung et al. 2005), but their spatial localization is only poorly assessed and it lacks cellular correlates. These problems are significantly diminished when using intracerebral local recordings, because the signals are generated in the volume surrounding the array of recording sensors. The parallel arrangement of principal cells and the pronounced stratification of inputs in the hippocampus also favor the application of ICA and interpretation of the results obtained.

Our recent application of ICA to LFPs in the rat CA1 showed several dominant generators of LFPs, producing a subcellular definition of their spatial localizations that was constant across animals (Makarov et al. 2010). A causal relation between the firing of local units and the activity of specific LFP-generators was also shown. This result suggests that each isolated LFP-generator may have a neuronal origin with dif-

* A. Korovaichuk, J. Makarova, and V. A. Makarov contributed equally to this work.

Address for reprint requests and other correspondence: O. Herreras, Cajal Inst.-CSIC, Av. Dr. Arce 37, Madrid 28002, Spain (E-mail: herreras@cajal.csic.es).

ferent functionality. Indeed, one may expect that the activity of an afferent input to a restricted dendritic field in the principal cells may be associated with a single LFP-generator disentangled by ICA from the complete LFPs. To test this hypothesis, here we have used selective electrical stimulation of known hippocampal pathways such as the Schaffer input to CA1 and the perforant path (PP) input to the dentate gyrus (DG). Selective stimulation elicits evoked LFPs whose well-known spatial maps are used to crosscheck the ICA-derived LFP-generators in the first part of the study.

Hippocampal evoked potentials are regularly used to explore the functional properties of neuronal populations. Experimental and theoretical studies show they are reliable population indices of the corresponding membrane events in single neurons (Andersen et al. 1971; López-Aguado et al. 2002; Varona et al. 2000). Evoked synaptic inputs produce inward and outward currents covering the entire morphology of principal cells with pathway specific spatial distribution that can be precisely determined by current-source density (CSD) analysis (Freeman and Nicholson 1975; Lorente de Nó 1947). As a first step, we assessed the spatial and temporal performance of the ICA, as well as its capacity to discriminate different sources using evoked LFPs of known origin.

Subsequently, we studied spontaneous LFPs primed by random sparse subthreshold evoked activity to identify the disentangled components. The presence of evoked and well-known spontaneous events specific for each pathway in the raw LFPs, and in a single LFP-generator, guarantees its correct unequivocal identification. We further quantified the specific contribution of LFP-generators to the global signal during irregular LFP patterns. Interestingly, the two major excitatory pathways, Schaffer and PP, contribute little to ongoing LFPs, producing scarce and irregular bouts of activity.

METHODS

Experimental methods

Female Sprague-Dawley rats (200–220 g) were anesthetized with urethane (1.2 g/kg, ip) and fastened to a stereotaxic device, maintaining their body temperature at 37°C with a heated blanket. The surgical and stereotaxic procedures performed were described elsewhere (Canals et al. 2005; Makarova et al. 2008). Concentric bipolar stimulating electrodes were placed in at least two of the following locations: the alveus for antidromic activation (from bregma, midline, and cortical surface AP: −5.5, L: 2.6, V: −1.8 mm), the ipsilateral CA3 (septal pole) for orthodromic activation of the CA1 region (AP: −3.2, L: 2.6, V: −3.3 mm), and the angular bundle (AP: −8, L: 4–5, V: 3.5–4 mm) for orthodromic activation of the granule cell population in the DG. These points were approached at a 30° angle in the sagittal plane. Stimuli (0.07–0.1 ms square pulses, 0.1–0.8 mA) were applied to elicit the characteristic evoked potentials, which were used to guide the placement of recording probes. Linear multisite probes (models: A1x16-5mm50-177 and A1x32-6mm50-413, Neuronexus Technologies, Ann Arbor, MI) were lowered into the hippocampus (AP: 4.5–5.5, L: 2–3 mm) and connected to a multiple high-impedance headstage. The 16-site probes were used to record along the main axis of CA1 pyramidal cells, whereas the 32-site probes spanned both CA1 and DG/CA3 regions. A silver chloride wire in the neck skin served as a reference for recording, and the signals were amplified and acquired using low-noise MultiChannel System (Reutlingen, Germany) recording hardware and software (50 kHz sampling rate). All the experiments were performed in accordance with European Union guidelines (86/609/EU) and Spanish regulations (BOE 67/8509-12 1988) regarding the use of laboratory animals.

Histology

Silicon probes were labeled with DiI (Molecular Probes, Invitrogen, Carisbad, CA) by soaking in a 1% solution of *N-N*-dimethylformamide (Sigma-Aldrich, St. Louis, MO). At the end of the experiment, animals were perfused transcardially with saline/heparine and paraformaldehyde (4%). Coronal cryostat sections (15 μm) were obtained and labeled with bis-benzimide (Sigma), and they were examined under a fluorescence microscope (560–610 nm) to identify the probe position (see example in the Supplementary Fig. S1).[1]

Independent component and current source density analyses of LFPs

The mathematical procedure and detailed signal treatment of the ICA were described elsewhere (Makarov et al. 2010). Briefly, 16 or 32 LFP signals $u(t) = \{u_k(t)\}_{k=1}^{K}$ recorded simultaneously can be represented as the weighted sum of the activities of N neuronal sources or LFP-generators[2]

$$u(t) = \sum_{n=1}^{N} V_n s_n(t) - \sigma \Delta V_n = I_n \; \forall \; n \in [1, N] \qquad (1)$$

where $V = [V_1, V_2 \ldots, V_n]^T$ is the mixing matrix composed of the so-called voltage loadings or spatial weights of all LFP-generators; $\{s_n(t)\}_{n=1}^{N}$ are the time courses or activations of the LFP-generators; σ is the conductivity of the extracellular space; and $\{I_n\}_{n=1}^{N}$ are the CSD loadings. Thus the raw LFP observed at the kth electrode tip is a linear mixture of the electrical activity of several independent LFP-generators describing transmembrane currents in principle cells.

Figure 1*A* shows an example of (evoked) LFPs recorded in the CA1 by a 16-site probe along the pyramidal neuron axis. The raw LFPs can be used to evaluate CSD maps by approximating the Laplace operator by 1D finite differences (Fig. 1*B*)

$$CSD = -\frac{1}{\sigma}\Delta u = -\frac{u_{k-1}(t) - 2u_k(t) + u_{k+1}(t)}{\sigma h^2} \qquad (2)$$

where $h = 50$ μm is the intersite distance. The CSD shows the characteristic Schaffer-evoked pattern, where several neuronal events can be appreciated overlapping in space and time, such as generation of a propagating population spike.

The ICA of $u(t)$ returns the generator's activation $\{s_n(t)\}_{n=1}^{N}$ (Fig. 1*C*) and the mixing matrix V (Fig. 1*D*) for ≤16 LFP-generators. Usually only a few of them (G1–G6 in the figure) have significant amplitude and different spatial distributions (voltage loadings). We noticed that, because of the ambiguity of the ICA (fortunately insignificant for our study), the voltage loadings and activations are given in arbitrary units (i.e., we can arbitrarily scale the loadings but we must simultaneously apply inverse scaling to the activations). Once LFP-generators have been extracted from the raw LFPs, we can analyze them as if they were active alone. For example, we can construct virtual LFPs produced by a single generator, say kth, from its voltage loading and activation

[1] The online version of this article contains supplemental data.

[2] Clarification of terminology. The term *source* is used with different implications in ICA and CSD analysis. In the former, source is used in a comprehensive manner to denote active brain regions (i.e., large zones of neural activity). Here a source in the ICA sense refers to each of the individual coherent components of the LFPs. Neither of these should be confounded with the formal notation of outward transmembrane currents or current sources used in CSD analysis. For the sake of simplicity, we maintain the latter and adopt the term LFP-generator for the ICA-derived sources.

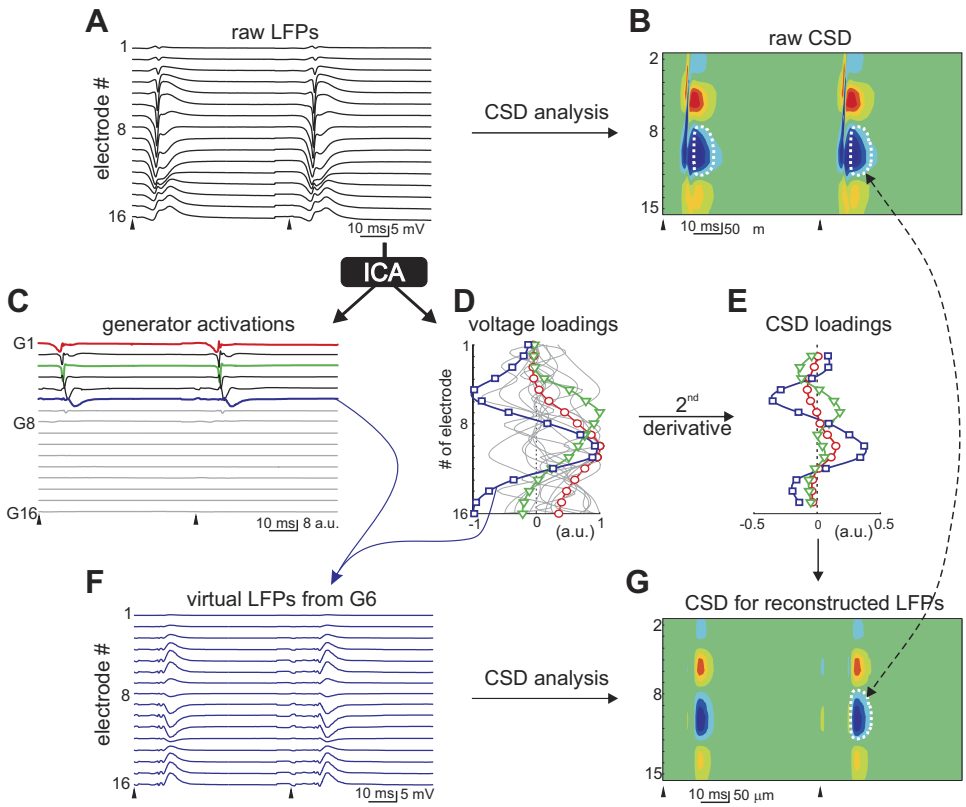

FIG. 1. General strategy of local field potential (LFP) decomposition and the identification of generators. The diagram shows the sequential steps from an LFP spatial map recorded along the CA1 axis containing evoked responses to a twin pulse in the ipsilateral CA3 (Schaffer response). A similar procedure is followed for spontaneous LFPs. The simultaneous recording of 16 sites along the main axis of the principal cell (pyramidal neurons) (*A*) is analyzed by current-source density (CSD) (*B*) to obtain the map of inward and outward population currents (sinks are in blue and sources in yellow-red). Multiple membrane events overlap spatiotemporally. The LFP profile is also analyzed by an independent component analysis (ICA) that provides a set of 16 generators each with a temporal activation (*C*) and spatial distribution (*D*). Of the 16 generators, only a few (1–6 in the example) have a significant variance, whereas the others are rejected for analysis. The second spatial derivative of the spatial weight curves (or voltage loadings) provides the CSD loadings (*E*), a spatial index that reflects the distribution of membrane currents along the conductor. Because the ICA does not ensure the correct polarity or absolute values of amplitude, we reconstructed the LFP for each generator isolated (*F*). Such partial LFPs regain the correct polarity and true amplitude. A CSD can be applied to the reconstructed LFP, which provides simplified spatiotemporal maps of inward/outward currents for unique spatially coherent membrane events (*G*). These maps can be compared with the CSD of raw LFPs (curved dashed arrow) to find specific membrane events buried within the mixed CSD (closed dashed white lines). It can be shown that the spatial profiles of partial CSDs (*E*) match the spatial profile of the CSD loadings (small dashed arrow) and hence their true polarity is assessed. Arrowheads mark the time of stimulus (artifacts have been removed for analysis). a.u., arbitrary units.

$$u_{G_k}(t) = V_k s_k(t) \tag{3}$$

Figure 1*F* shows LFPs contributed by G6 only. Note that the ICA ambiguity does not affect the virtual LFPs, i.e.: the reconstructed LFPs are dimensional. The virtual LFPs can be used to evaluate the CSD created by a single generator (Fig. 1*G* shows the CSD of G6), and thus the raw and generator-based CSDs can be compared (Fig. 1, *B* and *G*). We also noticed that, using *Eqs. 1–3*, the CSD related to the *k*th generator can be evaluated by $CSD_{G_k} = I_k s_k(t)$.

For the ICA, we made use of the infomax algorithm proposed by Bell and Sejnowski (1995) and further modified by Amari et al. (1996) and Lee et al. (1999). The algorithm is implemented in the EEGLAB Matlab toolbox (Delorme and Makeig 2004).

Comparison of LFP-generators: Distance measure

Each application of the ICA on LFPs, to either different recordings or for different time windows, provides several LFP-generators, and thus we need a method to compare and classify them. Each generator is characterized by its activation $s_k(t)$ and spatial loading V_k (Fig. 1, *C* and *D*). Activations are time specific and therefore they cannot be used for comparison. In contrast, the loadings depend on the spatial distribution of an axon's terminals and hence they must be similar for LFP-generators corresponding to the same population of presynaptic neurons. Thus to define a measure of similarity between a pair (*k*, *m*) of LFP-generators, we used the distance measure between their voltage loadings (Makarov et al. 2010)

$$d(V_k, V_m) = 1 - \frac{|\langle V_k, V_m \rangle|}{\|V_k\| \, \|V_m\|} \tag{4}$$

$$\langle V_k, V_m \rangle = \int_\Omega V_k V_m + \kappa \nabla V_k \nabla V_m + \kappa^2 \Delta V_k \Delta V_m dx, \; \|V_k\|^2 = \langle V_k, V_k \rangle$$

where $\kappa = 0.05$ mm^2 is the dimensional constant. The distance measure is bounded $0 \leq d \leq 1$ and $d = 1$ for two orthogonal (completely different) loadings, whereas $d = 0$ for two equivalent (identical) loadings.

To partition a set of voltage loadings into disjointed clusters, we use hierarchical clustering based on the introduced distance measure with the average-linkage algorithm.

Identification of stable LFP-generators

An ICA may theoretically isolate as many LFP-generators as the number of LFP signals (16 or 32 in these experiments), yet obviously, only a few of them will be statistically significant and stable. For

example, in Fig. 1*C*, the first 6 generators have high amplitude and they are clearly related to the stimulus, whereas the other 10 may capture noise and therefore they may vary strongly from one recording to another. In our former study (Makarov et al. 2010), we considered those LFP-generators contributing >5% to the total LFP variance (power) as statistically significant. The number of reliable components that can be extracted in practice depends on many factors such as the particular region under study, the signal to noise ratio, and the relative strength and spatial extension of active components. Some neuronal populations (e.g., hippocampal pyramidal cells) fire very rarely (Ranck 1973; Thompson and Best 1989) and hence, the postsynaptic activity of their targets may contribute little to the total LFPs. In this study, we consider an isolated LFP-generator with the variance contribution <5% to be significant, as long as it is unequivocally related to a known pathway and provides a clean CSD spatial map (low noise and a flat baseline). To identify the most stable LFP-generators in spontaneous LFPs, we used the two-step algorithm (Makarov et al. 2010). First, we identified "global" generators through an ICA of a sufficiently long recording (tens of seconds). Second, we divided the same recording into short-term contiguous epochs (each 1 s long), and we applied an ICA to each of these segments. We expect that stable strong LFP-generators should be presented in all epochs, whereas noisy, unstable, temporal or weak generators will fluctuate, and hence, their spatial loading will differ from epoch to epoch. We identified those that are most stable over time by calculating the similarity measure (4) between the "global" and "local" generators.

Power of LFP-generators

Using *Eq. 3,* we reconstructed virtual LFPs corresponding to the generator G_k, and we defined the mean power of G_k (measured in mV^2) as

$$P_{G_k} = \max_{m\in[1,K]}\left(\frac{1}{T}\int_0^T u_m^2(t)dt\right) \quad (5)$$

where T is the time interval for averaging (about a few minutes in our experiments). To evaluate the evolution of the power of the generator's activations over time, we use the convolution with the appropriately scaled square kernel H

$$P_{G_k}(t) = \int H(t-\tau)s_k^2(\tau)d\tau \quad (6)$$

Analysis of evoked LFPs

Evoked LFPs were recorded for a series of stimuli of varying intensity (short, 0.1 ms, square pulses at a rate of 0.1–1 Hz), from a low subthreshold to supramaximal [i.e., producing maximal population spike (PS)]. The stimulus intensity was measured in units of the threshold intensity to evoke a PS and stimulus artifacts were removed, except where indicated. Each series of evoked LFPs was analyzed as one long signal containing either all stimuli or selected groups of evoked responses. Only the period of interest (40–50 ms) immediately after the stimulus was analyzed for each profile, and thus intermediate periods were removed off-line and the time windows containing responses were concatenated into a continuous unique signal. This procedure does not affect the applicability of ICA but rather improves its efficiency by increasing the relative variance of the signal of interest.

Priming of LFPs with evoked activity

To identify the presynaptic populations corresponding to LFP-generators, we stimulated known afferent pathways with random sparse subthreshold pulses. The rationale was that the minimal electric activation of a pathway emulates its spontaneous excitation. Therefore the evoked and spontaneous activities of a given pathway must have the same spatial distribution as defined by the axon's terminals. Thus two types of LFPs with the same spatial characteristics must be captured by one and the same LFP-generator, and hence the presence of evoked responses in the activation of the LFP-generator $s_k(t)$ assists in its identification. In preliminary experiments, we found that subthreshold (<0.5 × threshold) stimuli delivered at an average rate of 1 Hz do not significantly change the variance of the total signal. We also found that strong (near threshold and suprathreshold) evoked responses produce a complex mixture of components when analyzed by ICA/CSD (see Fig. 1). Apparently such phenomena are not present in the low-amplitude events of ongoing LFPs, and thus we chose low stimulus intensities to prevent the generation of PS components (i.e., we achieve vanishing recruitment of intrinsic currents into field excitatory postsynaptic potentials (fEPSPs) during synchronous activation, Herreras 1990). For Schaffer activation, we chose stimuli that produced fEPSPs of ≤0.5 mV in the stratum radiatum, and for the PP input, the intensity was adjusted to raise a positive field in the Hilus ≤1 mV (below 0.5 mV in the DG molecular layer). To analyze the LFPs, we used a two-epoch recording: *1*) spontaneous and *2*) spontaneous plus evoked activities. Thus we can examine whether evoked activity modifies the level of spontaneous activity on the same or another LFP-generator. In accordance with the stability analysis of the LFP-generators (Makarov et al. 2010), we found that mixing sparse subthreshold evoked activity into ongoing LFPs neither modifies their characteristics nor affects the spatial profiles of the LFP-generators, as long as the probe array remained in place.

Reconstruction of LFPs for specific pathways

Reconstructed LFPs recover the correct polarity and provide a good quantitative estimate of the pathway-specific variance and power. The power was calculated in the electrode that showed maximum amplitude during irregular LFP patterns (i.e., excluding theta periods) over a total of 3 min of 20 s randomly chosen segments within 1 h. A major advantage of pathway-specific LFPs is that they provide simplified CSD maps describing a unique spatial structure of inward and outward currents. These can easily be matched to those obtained from customary hippocampal evoked fields, whose uncomplicated nature and well-defined distribution along the anatomy of principal cells assist path identification (Herreras 1990; Herreras et al. 1987; Leung et al. 1995; Lømo 1971).

RESULTS

We first tested the spatial and temporal performance of the ICA on evoked LFPs obtained by activation of the Schaffer-CA1 and PP-dentate inputs. Subsequently, we used the pathway specificity of the ICA-derived LFP-generators to explore the spontaneous population activity of these pathways in ongoing LFPs.

Spatial and temporal precision of pathway-specific LFP-generators

SEPARATION OF ARTIFACTS AND NEURAL ACTIVITY. The capacity of the ICA to suppress EEG artifacts is well established (see Castellanos and Makarov 2006; Vigario et al. 2000 and references therein), and thus we assess here its applicability to isolate stimulus artifacts (caused by electric shock) in deep brain recordings. We antidromically stimulated the CA1 pyramidal population from the alveus (Fig. 2*A*, *cartoon inset*), and the electric shock produced a large negative spike-like potential (>40 mV, truncated at the black dot in Fig. 2*Aa*) that may reverse polarity outside the hippocampal tissue. This artifact was followed by evoked LFPs with the characteristic profile of

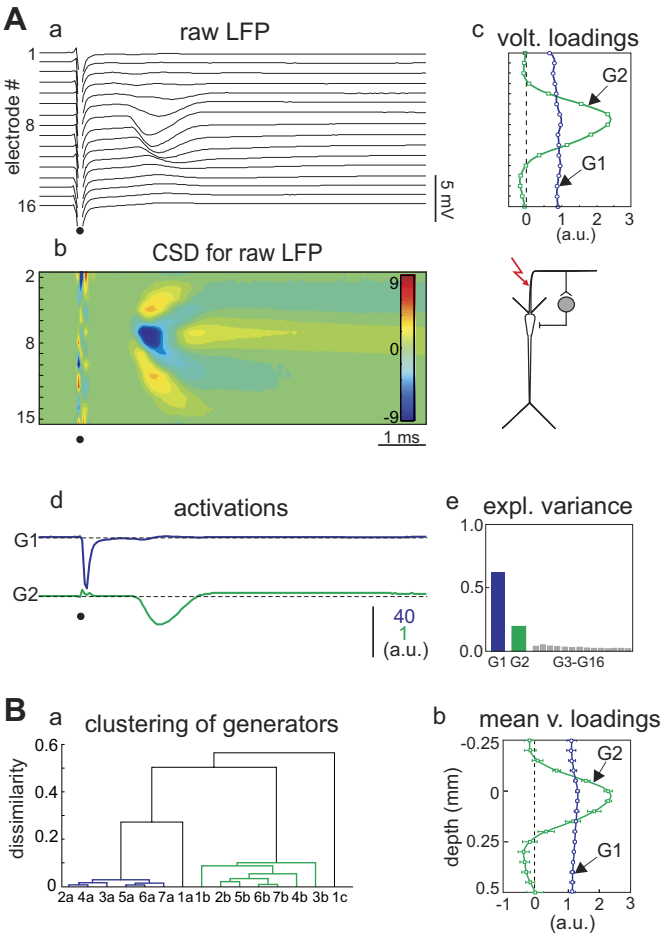

FIG. 2. Segregation of artifacts and neural activity by the ICA. The figure corresponds to the analysis of an LFP obtained during antidromic activation of the CA1 field. The alvear electric shock produced a large voltage artifact (dot in *Aa*) followed by an antidromic population spike. The artifact is nearly deleted in the corresponding CSD (*Ab*) while locally generated active sink and passive sources are visible. The ICA showed only 2 significant generators (*Bb*). G1 contains the stimulus artifact (*Ba*) that enters all electrodes with similar weight (flat voltage loading in *Ab*). G2 contains all the neural activity, displaying a bell-shaped voltage loading curve spanning the activated somatodendritic domains (*Ac*). *B*: the cluster analysis of all voltage loading curves obtained in 7 animals establishes 2 groups (blue and green) corresponding to the artifacts and population spikes, respectively. The average spatial loading curves is shown in *Bb* (mean ± SD).

the antidromic PS (Varona et al. 2000). The corresponding CSD map (Fig. 2*Ab*) shows the somatodendritic sink (blue, electrodes 7–11) surrounded by passive sources (yellow/red). The polarity of currents reverses in the ensuing slower tail, as expected for somatic recurrent inhibition (active somatic currents flanked by passive basal and apical dendritic currents).

The ICA successfully isolated the artificial potential as a single generator, G1, that was devoid of neuronal activity (Fig. 2, *Ac* and *Ad*, blue curves). We noted that the spatial voltage loading of the artificial generator is essentially flat (Fig. 2*Ac*, blue line). Such a generator, which enters all electrodes at the same strength or with a linear decay, has a null CSD (*Eq. 2*), which means that its origin lies outside the recording zone and that the generator is volume propagated, as expected. The second strongest LFP-generator, G2, contains the main part of the neuronal activity, including the PS and inhibitory currents. The LFP variance explained by the remaining G3–G16 is <5% (Fig. 2*Ae*). Thus when evoked LFPs contain a large artifact, the resolution of the mixed neuronal activity significantly deteriorates. Hence, in subsequent analysis, we routinely cut off the stimulus artifacts before applying the ICA.

We found that the results shown in Fig. 2*A* were stable in all animals, and the clustering analysis of voltage loadings of all the LFP-generators in the seven animals provided a well-defined partition into two groups (Fig. 2*Ba*; intracluster distance <0.15, intercluster distance >0.5). This is evident in Fig. 2*Bb*, which shows the mean ± SD spatial loadings for the artificial G1 and neuronal G2 generators averaged over loadings belonging to the corresponding cluster ($n = 7$).

SUBTHRESHOLD ACTIVATION OF AN AFFERENT PATHWAY IS CAPTURED BY A SINGLE LFP-GENERATOR WITH PRECISE SPATIOTEMPORAL DEFINITION. Let us now examine the ICA performance on LFPs evoked by activation of Schaffer-CA1 and PP-DG inputs (a detailed description of evoked LFPs and their CSD analysis can be found in the Supplementary Fig. S1). We first studied the excitatory Schaffer input to the CA1 that was activated by subthreshold (0.5 × threshold) stimuli to minimize the secondary intrinsic currents (Herreras 1990). Figure 3*A* shows raw profiles of evoked LFPs and the corresponding CSD map. It can be appreciated a single active sink centered in the st. radiatum, surrounded by two passive current sources in the soma region and distal apical dendrites.

Application of the ICA identified 16 LFP-generators, and only 1 of them, G1, had statistically significant amplitude (Fig. 3*B*). The activation of G1 matches the time course of the raw LFP at the site of maximum amplitude (electrode 9 in Fig. 3*Aa*). G1 has a bell-shaped spatial distribution (Fig. 3*Bc*, blue curve) that is maximal in the apical dendrites, and its polarity reverses in the soma layer, in close correspondence to the spatial profile of LFPs calculated for the time instant marked by the arrow in Fig. 3*Aa* (Fig. 3*Bc*, black line). The spatiotemporal dynamics of the CSD obtained from the LFPs reconstructed from G1 matched the CSD map calculated from the raw LFP profile (Fig. 3, *Be* vs. *Ab*). We noticed that the three-layered source-sink-source distribution caused by excitatory synaptic and return currents was not decomposed by the ICA into three different components, but rather, it was explained by the single G1 LFP-generator. The transmembrane source/sink loop of current raised by a discrete patch of active membranes is contained within the shape of the spatial weights of the ICA-isolated LFP-generator (loading vector V_1 in *Eq. 1*).

Similar results were repeatedly obtained in five animals, and in a clustering analysis of the loading curves obtained in different experiments, the interloading distance was <0.1 for all generators (Fig. 3*Ca*). In one experiment, we obtained two significant generators: one of them (2a in Fig. 3*Ca*) had a similar voltage loading as that described above (Fig. 3*Bc*), whereas the other (2b in Fig. 3*Ca*) was significantly different. Hence, in this experiment, it would seem that some spontaneous LFP event of a different origin overlapped with the evoked activity, which was isolated into a separate LFP-generator. The mean ± SD voltage loading for the Schaffer synaptic input averaged over $n = 5$ experiments is shown in Fig. 3*Cb*.

In a representative experiment that examines PP-DG evoked responses (Fig. 4), subthreshold (0.5 × threshold) activation of the PP produced the expected negative LFP in the molecular layer of both blades and a strong positive potential across the

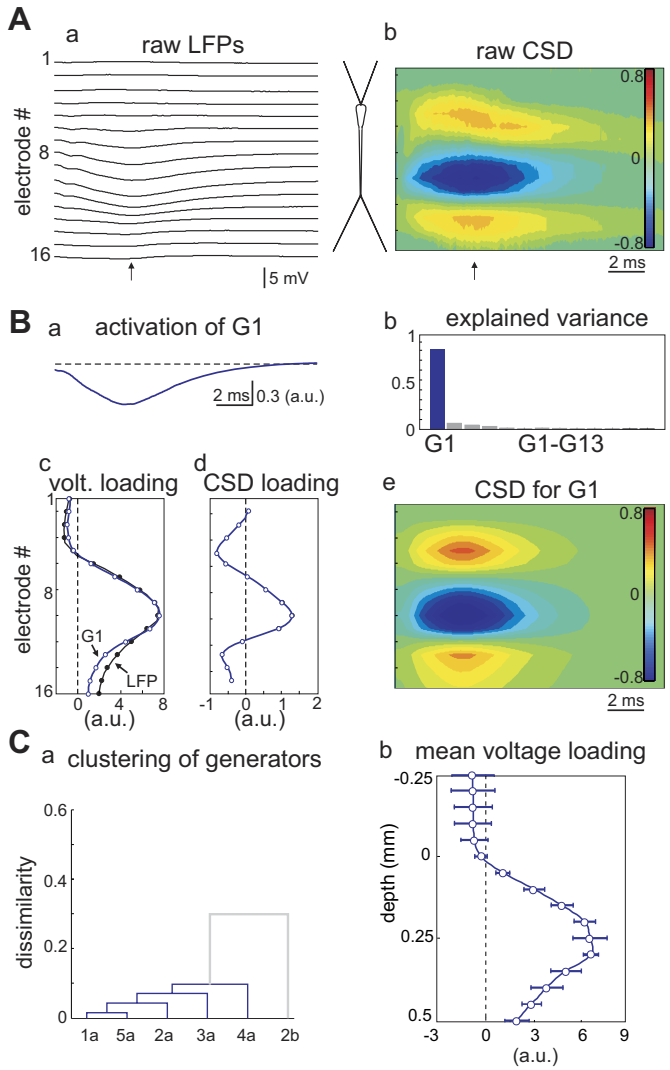

FIG. 3. Precise spatial and temporal performance of ICA on LFPs produced during subthreshold activation of the Schaffer input to CA1. *A*: an electric shock in the ipsilateral CA3 evoked a negative potential in the apical dendritic tree (*a*). The schematic neuron indicates the approximate recording position. The CSD reveals inward currents (sinks) centered in stratum radiatum flanked by passive sources in the soma layer and stratum lacunosum (*b*). *B:* the ICA applied to the LFP profile shows a unique significant component (*b*) with a temporal course matching the voltage change in central electrodes (*a*). *C*: the voltage and CSD loadings (blue plots) coincide with the spatial profiles of the raw LFP and CSD (black plots; measured at the instant marked by the small arrows in *A*). The CSD calculated for the reconstructed LFP for G1 (*c*) is similar to the raw CSD (*Ab*). *D*: cluster analysis for voltage loadings obtained in 4 animals show a unique group (*a*). The average voltage loading (mean ± SE) shown in *b* was built using the st. pyramidale as a spatial reference.

Hilus (Fig. 4*A*). The CSD map showed strong sinks in both molecular layers (*sk1*, *sk2*) and a weaker sink (*sk3*) produced by CA1 pyramidal cells in the st. lacunosum, in close correspondence to the known anatomical terminations of these fibers. Passive sources (return currents) appeared in the GCL (cartoon in Fig. 4*A*, *right*). The ICA of LFPs again rendered only 1 significant LFP-generator, G1 (activation in Fig. 4*Ba* and loading in Fig. 4*Bd*), whereas the other 15 were negligible (Fig. 4*Bb*). The CSD map of the virtual LFPs reconstructed for this unique generator (*Eq. 3*) matches the CSD of the raw signal (Figs. 4, *Bc* vs. *A*). Likewise the voltage and CSD loading curves (Fig. 4*Bd*) match the spatial profiles for the raw signals. Thus one ICA-isolated LFP-generator may contain synaptic activity from several separate populations, as long as they are simultaneously activated by a common input.

Qualitatively, the same results were observed when we repeated this analysis in five animals. However, since the separation between the GC layers varies because of the curved arrangement of this population, the anatomical normalization of the recording tracks across animals is not ideal. This precludes direct comparison of spatial loadings obtained in different experiments. Supplementary Fig. S2 shows the results from the other four experiments.

SEPARATION OF THE ACTIVITY EVOKED BY MULTIPLE PATHWAYS. Because of the volume propagation of extracellular currents, a LFP may contain activity from several domains within the same neurons or even from different distant populations and at a distance from the recording electrode. Thus we tested whether the ICA can decompose LFPs with a contribution from two pathways into the original Schaffer and PP inputs to the CA1 and DG, respectively.

Conveniently, the pyramidal and granule cell populations are spatially segregated, and they can be covered by different groups of electrodes in the 32-site linear probe. In the two representative experiments shown in Fig. 5, a series of subthreshold paired pulses of stimuli were delivered at a rate of 0.2 Hz rate to the Schaffer and PP pathways. These pathways were either stimulated with a 100 ms delay or simultaneously (*left* and *right columns* in Fig. 5, respectively). The stimulus intensity was maintained constant for the Schaffer input, whereas for the PP input, it increased over time for noncoincident pairs of stimuli (Fig. 5*A*) and decreased for the coincident pairs (Fig. 5*B*), yet always remained below a 0.5 × threshold. The LFPs recorded for the two stimulus configurations by the 32-site linear probe extended from the CA1 st. oriens to the lower GCL can be seen in Fig. 5*A* (see Supplementary Fig. S1 for greater detail).

NONCOINCIDENT STIMULI. An electric shock in the ipsilateral CA3 produces the Schaffer fEPSP in CA1, as well as a local multiphasic field in the CA3/DG. The CSD map shows the characteristic source-sink-source distribution of currents along the CA1 pyramidal cell axis and a local source-sink dipole (Fig. 5*B*, *Sch*). This latter dipole contains a mixture of the antidromic sink in the area of the granule cell and of the local recurrent orthodromic fEPSPs in CA3 (this local response may contain PP activation in other experiments, depending on the position of the stimulating electrode). Activation of the PP pathway produced an excitatory sink in the molecular layer (100 μm above the CA3 sink), as well as the corresponding somatic sources in both GCLs (Fig. 5*B*, PP). A weaker sink was also observed in the st. lacunosum of the CA1 region.

The ICA of the LFPs yielded three significant LFP-generators, G1–G3, with little if any cross-contamination (Fig. 5*C*). Noticeably, the time course of G1 activation shows increasing pulses in agreement with the increasing amplitude of the PP stimuli. In addition, the beginning of the G1 pulses coincides with the onset of the stimuli in this pathway. The other two LFP-generators, G2 and G3, exhibit pulses of constant amplitude (as for the Schaffer stimulation), whose onset coincide with the beginning of the stimulation to the Schaffer input. Thus the LFP-generator G1 exclusively represents the activity in the molecular layer of the DG (cf. Fig. 4), whereas the

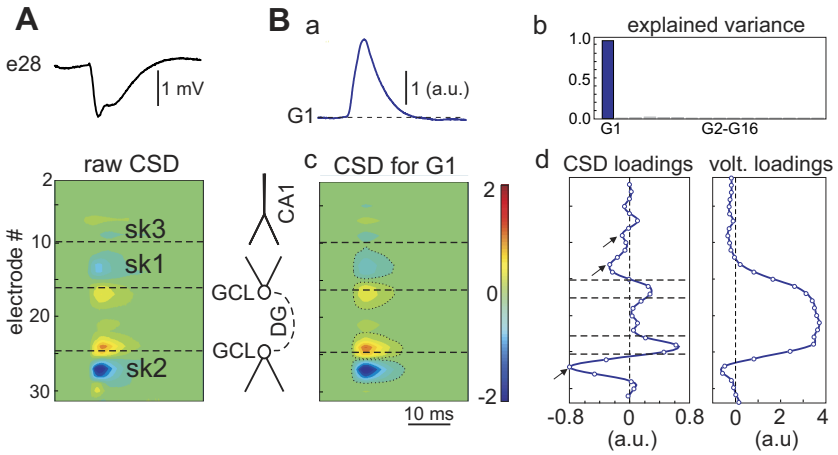

FIG. 4. Precise spatial and temporal performance of the ICA on LFPs produced during subthreshold activation of the entorhinal input to the dentate gyrus (DG). *A:* an electric shock in the ipsilateral perforant path (PP) evoked a negative potential in both molecular layers of the DG. A sample record from electrode 13 of a 32-site probe is shown in *a*. The raw CSD (*b*) shows active sinks in both molecular layers (*sk1* and *sk2*) and a weaker sink in the st. lacunosum of the CA1 (*sk3*). Passive sources can be appreciated in the granule cell layers (GCL). The schematic neurons show the approximate site of recordings. *B:* the ICA applied to the LFP profile shows a unique significant component (*b*) with a temporal course matching the voltage change in the molecular layer (*a*). The CSD calculated for the reconstructed LFP for G1 (*c*) is similar to the raw CSD (*Ab*). The voltage and CSD loadings (*d*) coincide with the spatial profiles of the raw LFP and CSD. Note that a unique ICA component captures coherent activity in physically separated cell generators as long as they are synaptically activated by a common input.

CA3-evoked LFPs were decomposed into two generators: G2 responsible for the Schaffer-mediated CA1 excitation (cf. Fig. 3) and G3 corresponding to the local CA3/DG activation. The CSD maps of the virtual LFPs reconstructed from each of the isolated generators (Fig. 5*D*) also confirm the pathway and population specific nature of the LFP-generators. Therefore ICA provides an accurate decomposition of multiple inputs that are not temporally coincident.

COINCIDENT STIMULI. In principle, the tight temporal coincidence of multiple sources decreases the efficiency of ICA to separate them. Thus we checked its performance on two precisely synchronized different inputs. When the stimuli were delivered simultaneously to the Schaffer and perforant pathways (Fig. 5, *right column*), there seemed to be a complex mixture of the sources and sinks in the raw CSD map. Notably, the proximity of the CA3 and GC layers led to fusion of their respective sinks into a unique slightly drifting sink (Fig. 5*B*), which made the sinks indistinguishable and complicated its direct interpretation.

Even in this case, the ICA still rendered three significant LFP-generators. Each of the generators had voltage loadings similar to those found in the noncoincident case (Fig. 5*C*, *left* vs. *right*), although their separation was less effective. As such, the strongest LFP-generator, G1, responsible for the PP input, introduced some contamination into the other two. This cross-contamination could be appreciated by comparing the loading curves in the *left* and *right columns*. We noticed that in the lower part of the loading curve (DG/hilus) for the Schaffer G2 (arrow pointing to red curve), there was a spatial weighting analogous (disregard the polarity) to that of the PP-specific G1 generator (arrow pointing to blue curve). The CSD maps for the reconstructed LFPs (Fig. 5*D*) show that the Schaffer-specific G2 generator contains some current belonging to the CA3 and FD regions (*left* vs. *right columns* in Fig. 5*D*). Nevertheless, even in this extreme case of the perfect time coincidence of different inputs, the specific activations of the LFP-generators confirm an adequate separation. Indeed, only G1 exhibits decaying amplitude of activation in agreement with the decaying intensity of the stimulus applied to the PP input, whereas G2 has stationary amplitude in agreement with constant stimulation of the Schaffer pathway. All these results were reproduced in four additional animals.

Schaffer and PP population activity in ongoing LFPs

We showed that ICA can separate Schaffer and PP evoked activities mixed in LFPs, and we described their spatiotemporal characteristics. Neither of the spatial weight curves (loadings) for these pathways matched those found in our former study, which described the most powerful generators in spontaneous LFPs (Makarov et al. 2010). This observation suggests that the LFP-generators describing the activity induced by the excitatory pathway may contribute weakly to the spontaneous LFPs. Thus we sought after the LFP-generators for the Schaffer and PP inputs in ongoing LFPs by mixing in subthreshold stimuli that facilitate the identification of the generators.

IDENTIFICATION OF SCHAFFER AND PP POPULATION ACTIVITIES IN ONGOING LFPS. A fragment of ongoing LFPs was analyzed during which both pathways were activated in a random-like manner at an average rate of 1 Hz each (Fig. 6*A*). The vertical dashed red and blue lines mark the onset of the Schaffer and PP stimuli, respectively. Because of the weak intensity of the electrical stimulation, the evoked responses are hardly discernible in the raw LFPs. By applying an ICA, we found five main LFP-generators (Fig. 6, *B* and *C*), two of which exclusively contain the evoked responses to the Schaffer (G2) and PP (G4) stimuli (Fig. 6*C*). We noticed that the activations of the other LFP-generators (G1, G3, and G5) did not correlate with the onset of the stimulus, indicating that there was little if any cross-contamination between these generators. The remarkable specificity of the activities contained within G2 and G4 (Fig. 6*B*) was proof that both are truly independent and well-isolated LFP-generators responsible for the Schaffer and PP inputs, respectively. The shape of the voltage loadings (spatial weight curves) for G2 and G4 are essentially identical to those found in experiments where only evoked activity was assessed (cf. Fig. 6*C*, red and blue curves to Figs. 3*Bc* and 4*Bd*, respectively, and also to Fig. 5*C,* red and blue curves). The portion of the variance explained by the two primed pathways (bars in red and blue) is small (<5%; Fig. 6*D*). This reduced contribution of the Schaffer and perforant pathways to LFPs makes their identification in ongoing spontaneous LFPs extremely difficult. As such, LFP-generators containing their activities fall below the level of significance and hence they can be overlooked.

RECONSTRUCTION OF PATHWAY-SPECIFIC LFPS AND THEIR SUBCELLULAR SPECIFICATION. Disentangling the raw LFPs into LFP-generators enables the reconstruction of virtual LFPs produced

by a specific pathway during ongoing activity and their separate analysis. An example is shown in Fig. 7 for an LFP fragment containing three evoked (subthreshold) pulses (applied to Sch or PP pathways; the onset of each is marked by a dashed line in Fig. 7*A*). The LFP was recorded from the pyramidal/oriens border in CA1 to the lower blade of the DG. The corresponding CSD map shows a confusion of sources and sinks produced by the ongoing spatiotemporal activity of different origins (Fig. 7*B*).

The ICA of the LFP fragment rendered five LFP-generators (Fig. 7*C*), and their spatial loadings and time course of activation can now be used to identify pathway-specific evoked activity. By searching for the evoked responses among all generators and comparing their activations and voltage loadings to those shown in Fig. 6, *B* and *C*, respectively, we identified G2 and G4 as responsible for the Schaffer and perforant inputs, respectively. Because of the ambiguity of the ICA (see METHODS), the time course of the activations is given in arbitrary units and is not directly comparable. However, we can reconstruct the virtual LFPs created by each single generator. Figure 7*D* shows LFPs reconstructed for the Schaffer generator (G2). The spontaneous population activity and two of the evoked events can be tracked down in the raw signal. The reconstructed evoked potential profile shows no difference to its raw counterpart, as expected (see the ellipses in Fig. 7, *A* and *D*, amplified in the *right insets*). By visual inspection of the raw and Schaffer reconstructed LFPs, it is patent that ongoing raw LFPs are most prominent in the hilus of the DG (lower electrodes), whereas Schaffer mediated activity is more conspicuous in the CA1. Also some activity in the CA3/DG region that is probably caused by recurrent excitation of presynaptic pyramidal cells in the CA3 region.

As further confirmation of the specificity of the Schaffer generator (G2) identified, we compared its activation (Fig. 7*B*, G2) with the high-frequency activity (~100–200 Hz) associated to sharp waves, an electrographic event known to be caused by synchronous activation of the CA3 region (i.e., Schaffer-mediated: Buzsáki et al. 1983). Indeed, the specific bouts of activity contained within the Schaffer G2 generator were coherent with ripple-like fast activity in the CA1 perisomatic LFPs (black top trace in Fig. 7*B*; band-pass: 100–500 Hz).

To obtain the precise localization and magnitude of the underlying transmembrane currents, we evaluated the CSD of the reconstructed LFPs (Fig. 7*E*). As expected, the Schaffer population activity presented a main sink in the st. radiatum surrounded by passive sources (return currents) in the st. pyramidale and lacunosum, matching the locations of the well-known CSD map for evoked Schaffer activity (Fig. 3). The CSD maps of isolated pathway-specific LFPs contrasted with those obtained for the mixed signal (cf. Fig. 7, *B* and *E*). It is worth mentioning that the temporal activation of isolated components corresponds to that of the population synaptic currents (e.g., compare the evolution of the CSD map at

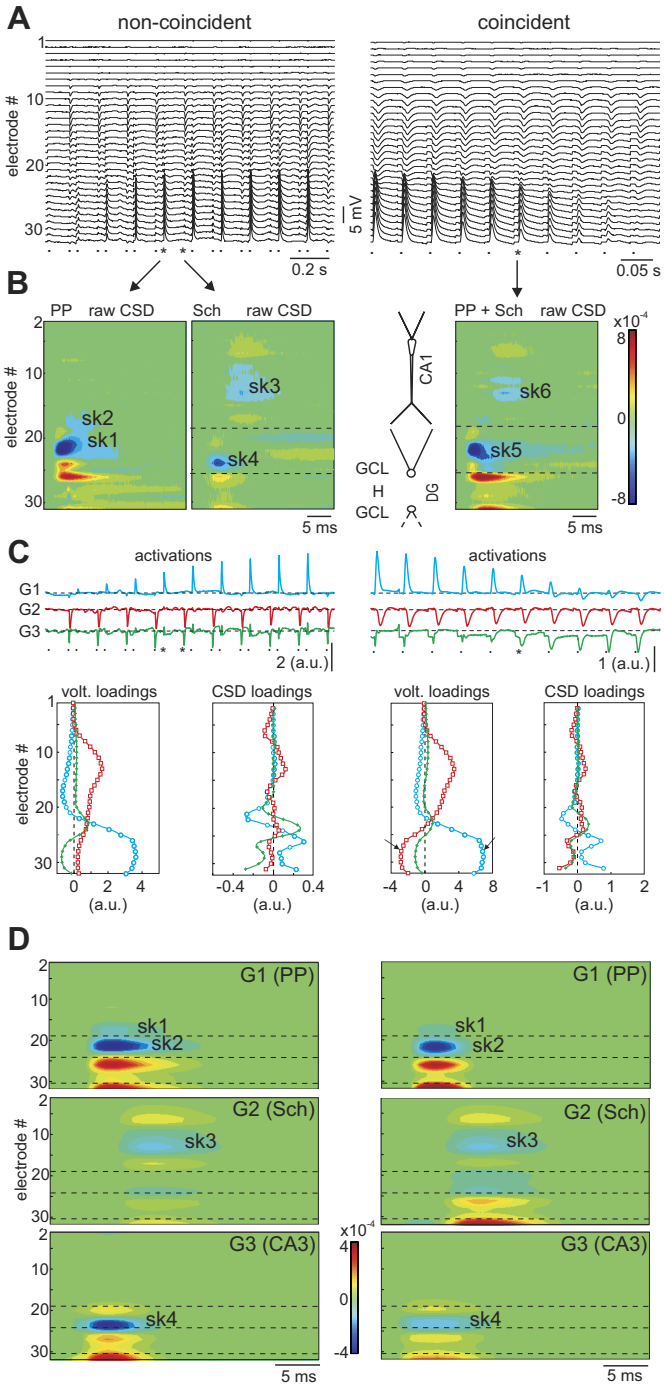

FIG. 5. Discrimination of multiple evoked synaptic inputs in mixed LFPs. Subthreshold stimuli were applied to both the ipsilateral CA3 (Schaffer) and the PP, either as paired pulses (100 ms delay, *left column*) or synchronously (*right column*). PP stimuli were modulated in intensity, whereas CA3 stimuli were constant. *A*: raw LFPs recorded along a track spanning the CA1 and CA3/DG up to the lower GCL. *B*: CSD maps for a sample response (raw CSD) to either the PP, the CA3 (Sch), or both. Schematic neurons between panels show the approximate locus of recording. PP produced a main sink in the st. moleculare (*sk1*) and a weaker sink in the CA1 st. lacunosum (*sk2*). CA3 activation raised a sink in the CA1 st. radiatum (*sk3*) and a local sink (*sk4*). Combined stimuli produced a complex sink in the DG (*sk5*) and the Schaffer sink in CA1 (*sk6*). *C*: the ICA yielded 3 significant generators in both cases. G1 and G2 correspond to the PP and Schaffer generators, respectively, whereas G3 corresponds to local activity in the CA3/DG. The top traces show the time activation and the bottom traces show the corresponding spatial voltage and CSD loadings. Note that activations vary in G1 with successive stimuli, whereas they remain constant in G2, precisely reflecting the intensity applied in each case. The spatial loadings for G1 and G2 were identical as when each pathway was stimulated alone. A small contaminant appeared during coincident stimulation (small arrows). *D*: virtual CSD maps for sample responses of each separate generator. Note the spatial coincidence of the separate virtual sinks with those in the raw LFPs.

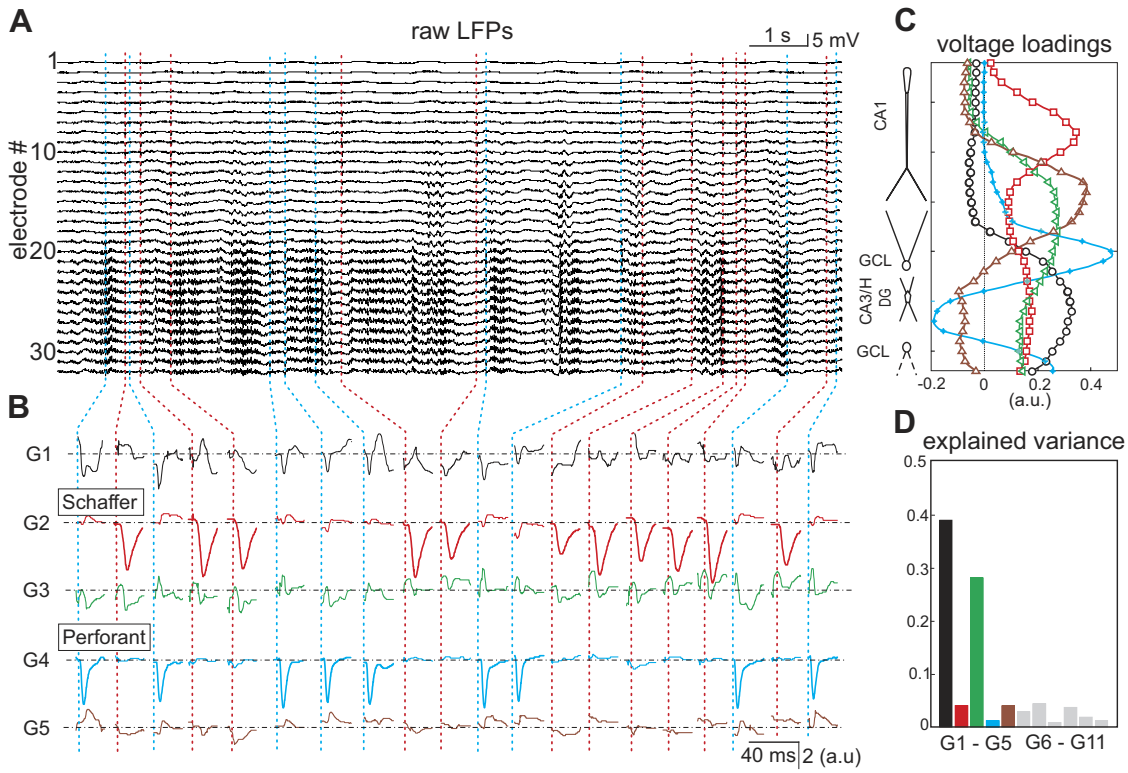

FIG. 6. Identification of the Schaffer and PP population activities in ongoing LFPs. *A*: segment of raw LFPs recorded from the CA1 st. pyramidale to the lower GCL in the DG. LFPs were primed with subthreshold stimuli applied in a random manner to the CA3 (Sch) and PP. The vertical dashed lines mark the timing of stimulation (blue for PP and red for CA3). Evoked potentials are short and small, and hence, they do not introduce much variance in the raw signals (they are hardly discernible over this time scale). *B–D*: the ICA yielded 5 principal generators, 2 of which specifically contain the activation corresponding to the evoked potentials for the Schaffer (G2) and the PP (G4). *B*: an amplification of the responses after each stimulus. Note the pathway specific segregation of evoked responses in the corresponding generators. The spatial loadings shown in *C* match those found for nonprimed LFPs (G1, G3, G5) or for separately stimulated pathways (G2, G4). *D*: relative variance of the generators isolated.

electrodes 8–9 in Fig. 7*E* to the corresponding activation in Fig. 7*C*, red trace). Thus LFP-generators isolated by the ICA enable the population-specific transmembrane current density to be examined, rejecting contamination of the other inputs in ongoing LFPs.

MINOR CONTRIBUTION OF EXCITATORY PATHWAYS TO HIPPOCAMPAL LFPS. The Schaffer and PP generators (G2 and G4) identified that describe the activation of the corresponding pathways enabled the spontaneous activity of these pathways to be studied and quantified (i.e., the presynaptic CA3 and entorhinal afferent populations, respectively). In general, we found that the spontaneous activity (during irregular LFPs) of both the Schaffer and PP generators represents an irregular pattern of short bouts over a rather flat baseline. These can be appreciated in a sample epoch in Fig. 8*A* along with their respective wavelet spectra. They lasted a few hundred milliseconds, had variable amplitude and occurred at <1 Hz rate. Smaller and shorter events can also be appreciated, which may be physiologically relevant. The main frequency content of the activity concentrates in the 0.5–4 Hz range for both generators. To track the evolution of the generator's power over time, we calculated time envelopes of this activity (see METHODS and *Eq. 6*), where large events and baseline activity can be better distinguished (Fig. 8*B*).

The dimensional power (measured in mV^2) that contributed to the ongoing LFPs for each synaptic pathway can be estimated from the virtual LFPs reconstructed from the corresponding LFP-generators (see METHODS and *Eqs. 3* and *5*). The Schaffer and PP inputs produce 0.045 and 0.031 mV^2 on average (7 and 5% of the total power), respectively (Fig. 8*C*), whereas the contributions of the other generators ranged between 0.13 and 0.24 mV^2 in four animals. This result corroborates the relatively small contribution of the excitatory pathways into the total LFP variance observed above (Fig. 6*D*), but now excluding the evoked activity. We also noticed that the powers of the Schaffer and PP generators have smaller SE relative to the powers of G1, G3, and G5, which suggests that the Schaffer and PP inputs described are more stationary in time and between different animals than the other three LFP-generators.

DISCUSSION

Studying the mechanisms of neural information processing requires certain knowledge of the circuitry and of the causal and functional associations between activities of different neuronal groups. Here, we showed that an ICA can effectively separate standard LFPs in the hippocampus into pathway-specific isolated activities, called LFP-generators, describing the inputs of multiple presynaptic populations. The main requisite for the separation is the different spatial distribution of transmembrane currents along the somatodendritic axis of principal cells, whereas the temporal pattern of the pathway's activation is less important (e.g., they can be rhythmic or irregular).

Using selective subthreshold electrical activation of major excitatory synaptic pathways, such as the Schaffer and PP inputs, we described spatiotemporal features of LFP-generators specific to each. Subsequently, the Schaffer and PP generators found were used to quantify the pathway-specific contribution to ongoing LFPs. Hence we have consistently shown in all studied animals that the contribution of the major excitatory pathways to the power of ongoing LFP signals is minor (~7 and 5%, respectively). We also showed that both Schaffer and perforant pathways have irregular temporal patterns, with bouts of population activity of varying amplitude and with the frequency concentrated in the 0.5–4 Hz range.

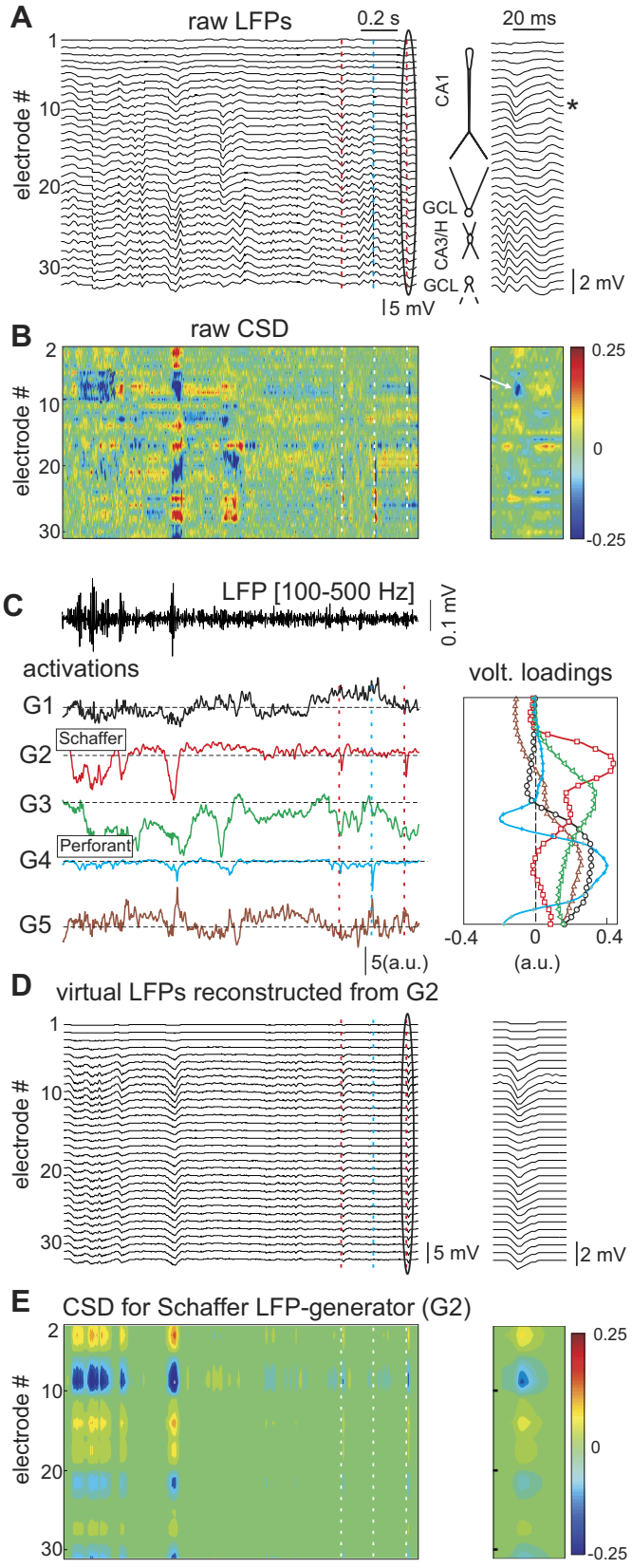

FIG. 7. Characterization of pathway-specific activity in ongoing LFPs. *A*: segment of raw LFPs recorded from the CA1 st. pyramidale to the lower GCL in the DG. The CA3 and the PP were stimulated to prime LFPs with Schaffer and PP evoked activity (instants marked by red and blue dashed lines, respectively). The ellipse marks a Schaffer evoked response enlarged to the right. Note the subthreshold field excitatory postsynaptic potential (fEPSP) in the st. radiatum (electrodes 3–10, asterisk). *B*: CSD map estimated for the raw LFPs. Note the complex mixture of currents. The Schaffer sink in the evoked response is appreciated in the amplification on the right (small arrow). *C*: ongoing activities of the 5 main generators separated by the ICA. G2 and G4 correspond to the Schaffer and PP generators, respectively. Note the characteristic spatial voltage loadings on the *right*. The top (black) trace corresponds to the filtered (100–500 Hz band-pass) LFP recorded from the CA1 soma layer. Note that epochs of fast oscillations coincide with the bouts of activity in the Schaffer generator (G2), matching the features of sharp wave events. *D*: reconstruction of the Schaffer-specific LFP. This virtual LFP now contains only the virtual LFP corresponding to ongoing activation of the CA3 to CA1 input. The amplification on the *right* shows the virtual fEPSP for a sample Schaffer response. Note that all evoked and spontaneous activity undergo changes of identical polarity for a given electrode. *E*: virtual CSD map for the ongoing Schaffer activity. Schaffer evoked sinks and sources are now like the standard evoked responses (compare. with the raw CSD in *B*).

Methodological considerations

A critical consideration regarding the ICA is that the components found may have little functional relevance unless accurate information on their anatomical basis is provided. All the same, ICA can efficiently separate signals coming from distant point sources (Choi et al. 2005). There are few studies on ICA of deep brain recordings (Makarov et al. 2010; Tanskanen et al. 2005). In deep recordings, the signals generated in the volume surrounding the electrode array (i.e., the sources or LFP-generators) are essentially extended spatially, and their spatial scales may be larger than the interelectrode distance. However, the same mathematical principles are applicable to LFP recordings (Makarov et al. 2010). Disentangling such LFP-generators is based *1*) on the coincident activation of individual homologous fibers over the millisecond time scale and *2*) on their different spatial distributions. The first condition provides the necessary synchronization of homologous axons to raise significant macroscopic synaptic field potentials, the main contributors to normal LFPs (Mitzdorf 1985; Nunez and Srinavasan 2006). The second condition is ensured by the distinct distributions of afferent axons from different afferent populations. The accuracy of the spatial resolution is therefore optimized to the subcellular level of the active neurons. We showed that the spatial CSD-loading curves of the Schaffer and PP LFP-generators match the configuration of the inward and outward currents for known membrane events (Andersen et al. 1971; Herreras 1990; Kandel et al. 1961). Admittedly, some factors can modify the expected spatial pattern of field potentials, such as the heterogeneous electrical properties of the conducting medium, spatial cancellation, and frequency scaling of currents in the volume conductor (Bédard et al. 2004; López-Aguado et al. 2001; Makarova et al. 2008). In earlier

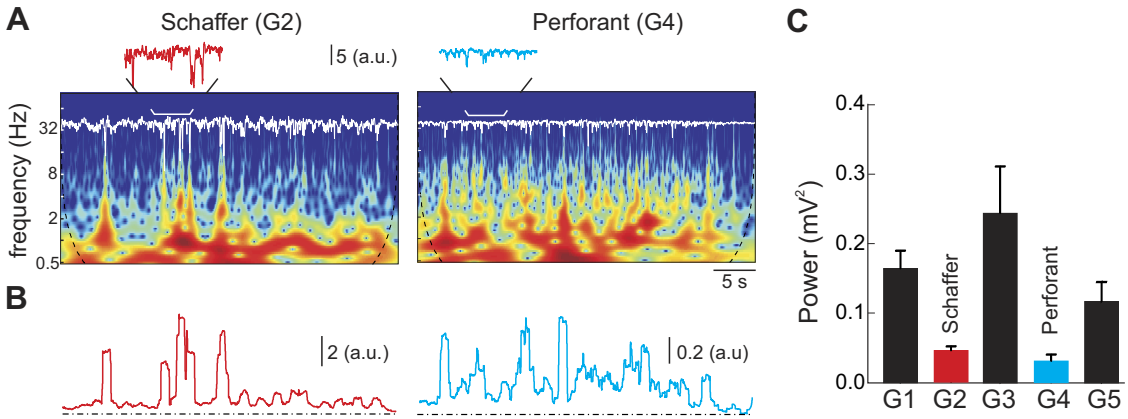

FIG. 8. Minor contribution of the excitatory generators to the hippocampal LFPs. *A*: frequency content of the ongoing Schaffer (G2) and PP (G4) generators during irregular activity in the raw LFP. The spectrogram shows dominant activity <2–3 Hz. The white trace shows the temporal activation of the generators (amplified above). The specific activity of spontaneous pathways was in both cases sparse and highly irregular. *B*: time envelopes of activity (1 s time window). *C*: average power of reconstructed LFPs for specific generators in 6 animals (mean ± SE) during irregular activity in the raw LFP. Note the small global contribution of excitatory generators.

experimental and modeling work, we reported some particular cases where some of these may be relevant (López-Aguado et al. 2001, 2002; Makarova et al. 2008; Varona et al. 2000). Such studies cannot easily be extrapolated on the distribution of LFP-generators. Because this analysis was performed on locally recorded LFPs, we speculate that the factor potentially most relevant is the mutual spatial cancellation between individual synaptic inputs when these are scattered through extended dendritic domains (Makarova et al. 2010). The excitatory Schaffer and PP inputs are strongly stratified; hence we would not expect a strong bias introduced by this factor either.

This approach is not dependent on the presence of rhythmic activity or stereotyped LFP events, and hence it can be applied to a wide variety of behaviors. Indeed, all the examples shown in this report were chosen among epochs of irregular activity, whose behavioral correlates are very rich (Jarosiewicz and Skaggs 2004).

In neuroscience, ICA is frequently used to suppress artifacts in EEG recordings (Castellanos and Makarov 2006). We showed that artifacts caused by electric shocks within brain tissue can also be isolated and suppressed by the ICA. However, strong artifacts (≤100 times higher than the neuronal activity) decrease the efficiency of the ICA for the simultaneous separation of other mixed components of neuronal origin. Hence we suggest that artifacts should be removed before performing an ICA.

The weak contribution of the Schaffer and perforant pathways to ongoing LFPs makes their identification extremely difficult (i.e., LFP-generators can be overlooked). Therefore we used selective low-magnitude electrical stimulation of the known excitatory pathways to ensure the reliable identification of LFP-generators describing the activity of these pathways. Thus the identification was based on *1*) a comparison of spatial voltage loadings of the LFP-generators found for evoked responses with those found for ongoing LFPs and *2*) the recognition of evoked pulses in the time courses of LFP-generators obtained by ICA of composite epochs (i.e., a recording consisting of 2 epochs: spontaneous LFPs and spontaneous plus a few evoked LFPs).

The polarity of the CSD loading is essential to define whether an LFP-generator describes excitatory or inhibitory input. However, the ICA cannot unequivocally determine this feature (Hyvärinen and Oja 2000). Although this problem is hard to solve for spontaneous LFPs and requires special biophysical assumptions (Makarov et al. 2010), we found that mixing sparse subthreshold evoked potentials in LFPs can be used to resolve the problem. The presence of evoked pulses in the time course of an LFP-generator is related to the stimulated neuronal population, and it helps identify the correct polarity. The subsequent application of CSD analysis on virtual LFPs reconstructed from a single generator enables the resultant partial CSD map to be directly compared with the raw CSD and with CSD maps of well-known evoked responses of specific pathways. It is worth noting that CSD map of isolated generators show no alternations in terms of the current's sinks and sources, as expected for a specific synaptic input. In contrast, raw CSD maps may contain such alternations because of the spatiotemporal mixing of the activities of several generators and DC filtering (Brankačk et al. 1993).

When and what can an ICA discriminate in LFPs?

To correctly interpret LFP-generators isolated by an ICA, it is relevant to ask whether each of them corresponds to postsynaptic activity from one or several neuron types. This problem is simplified greatly by the use of linear probes in the hippocampus where each subfield has only one type of principal cell: namely pyramidal and granule cells. Each synaptic input produces loops of inward/outward currents with a different spatial distribution within the same core conductor. Typically the maximum potential is attained at the center of the synaptic contact made by the isolated pathway (Herreras 1990). However, distant recording sites also contain activity, albeit of reduced magnitude. Therefore steadily correlated recording sites correspond to anatomical subdomains of one type of principal cell, whereas the subcellular precision can be achieved through a CSD analysis of the distribution of spatial weights in isolated generators. This procedure enables the separation of inputs into a single population according to known stratification along the dendritic arbor.

However, when linear recording probes extend through several subfields (e.g., CA1 and DG/CA3), the interpretation may not be that trivial because of volume propagation of currents and/or the simultaneous activation of populations in both subfields. The electrical fields created by two physically separated cells extend beyond their respective physical limits, mixing in local record-

ings. This is not a handicap for this approach because the temporal activation for each generator has no spatial dimension (i.e., it contains the coherent activity of a group of electrodes regardless of their location). Accordingly, the CSD examination shows whether the activity can be circumscribed to one or several physically separated cell generators. In this study, we found that the two excitatory generators seem to have true activity in more than one region. Thus the activity of the entorhino-hippocampal pathway (PP) was contained in only one LFP-generator, but it was divided between both blades of the DG. The parsimonious explanation is that the presynaptic population activates two or more physically separate target populations through bifurcating axons, in agreement with anatomical and electrophysiological findings (Hjorth-Simonsen and Jeune 1972; Lømo 1971). Hence, activation is identical and simultaneous in both blades, and thus it can be described by a single LFP-generator isolated by the ICA. With regard to the Schaffer generator, although CA3 activation rendered a single component in CA1 whose spatial loading curve matches the termination of Schaffer collaterals (Herreras 1990), prominent activity was also obtained near the stimulating electrode in the CA3/DG. The origin of this local activity varied somewhat in different experiments and was most commonly found in the molecular layers of the DG for evoked responses, probably because of backfiring of the PP fibers (Wu et al. 1998). During spontaneous LFPs, the CA3/DG activity associated to the Schaffer generator is less prominent, and it most likely reflects the synchronous activity of CA3 pyramidal cells because of recurrent excitation in this area (Miles and Wong 1987). Thus the CA3 pyramidal population is presynaptic for both CA1 and itself, and therefore the ongoing activity in the Schaffer generator should appear simultaneously in both regions, as happens to be the case.

Excitatory currents contribute little to hippocampal LFPs

Some LFP events and rhythmic oscillations have been studied intensively, and the neuronal circuits producing them have therefore been clarified. For example, sharp hippocampal waves are known to be mediated by the excitatory input from CA3 to CA1 populations (Buzsáki et al. 1983). Here, we also observed a correlation between sharp waves and the ICA isolated Schaffer generator describing the synaptic activity produced by CA3 pyramidal cells in CA1. Some LFP events, such as the theta rhythm, have a mainly inhibitory origin (Soltesz and Deschenes 1993), whereas others are still under study, such as gamma oscillations (Csicsvari et al. 2003; Mann et al. 2005), fast ripples (Ylinen et al. 1995), and dentate spikes (Bragin et al. 1995). In light of the proportion of excitatory and inhibitory neurons in the hippocampus (Aika et al. 1994), the small contribution of the major excitatory pathways to hippocampal LFPs might seem unexpected (Schaffer and PP generators explain 7 and 5% of the power, respectively). The other three LFP-generators show a significant phase-spike relationship, with ~60% of the putative interneurons in CA1 (Makarov et al. 2010), suggestive of their inhibitory nature (i.e., the corresponding synaptic currents are produced by local inhibitory circuits). Circumstantial data in the literature argue in favor of the dominance of inhibitory over excitatory currents in ongoing population activity (Hajos et al. 2000; Herreras et al. 1988; Oren et al. 2010), although direct evidence is scarce. The dominance of inhibitory currents was found in synaptic noise recorded from membranes of cortical pyramidal cells (Rudolph et al. 2005; see also Anderson et al. 2000; Borg-Graham et al. 1998). Besides the firing rate of several types of interneurons in the hippocampus is much higher than that of pyramidal cells (Somogyi and Klausberger 2005). Along with the functional coordination of some interneuron networks (Whittington et al. 1995), the hypothesis that inhibition prevails over excitation in hippocampal LFPs becomes more plausible. Nonetheless, the precise percentage of excitatory contribution to LFPs found here may vary in the freely moving animal, because anesthesia modifies the overall pattern of LFPs (Brankačk et al. 1993; Buzsáki et al. 1986).

In any case, the results presented here point to a very low output rate of CA3 pyramidal cells during irregular LFPs, in agreement with previous data (Ranck 1973; Thompson and Best 1989). In terms of the PP generator, the overall behavior was similar (occasional synchronous bouts of irregular activity), again indicating a low output rate from entorhino-hippocampal projection cells during irregular patterns of LFP. The presynaptic origin of this generator is suggested by the limited evoked responses after PP stimulation. The identity of the entorhinal projecting cells is not clearly established in the literature, and difficulties may arise from the fact that the entorhino-hippocampal projection is multifarious. Unitary studies have not clarified this issue, because most interest has focused on the relationship of entorhinal units with theta (Alonso and Llinás 1989; Chrobak and Buzsaki 1994; Frank et al. 2001). Thus stellate and pyramidal-like cells have been deemed candidates for this projection. Indeed, interesting functional data supporting the identity of the PP generator shown here is that the bouts of activity are not related to hippocampal sharp waves (Chrobak and Buzsaki 1994), which is consistent with the poor temporal correspondence between bouts of activity in the Schaffer and PP generators.

To conclude, we propose the combined use of ICA and CSD as a high-resolution method for the subcellular identification of LFP components in regular structures and for the quantification of their ongoing activity.

ACKNOWLEDGMENTS

We thank M. Sefton at BiomedRed for editorial support, S. Canals for critical reading and comments, and L. López-Mascaraque and N. Salvador for help with histological processing.

GRANTS

This work was supported by Spanish Ministry of Education and Science Grants BFU2007-66621/BFI and FIS2007-65173 and Comunidad Autónoma de Madrid Grant S-SEM-0255-2006.

DISCLOSURES

No conflicts of interest, financial or otherwise, are declared by the author(s).

REFERENCES

Aika Y, Ren JQ, Kosaka K, Kosaka T. Quantitative analysis of GABA-like-immunoreactive and parvalbumin-containing neurons in the CA1 region of the rat hippocampus using a stereological method, the dissector. *Exp Brain Res* 99: 267–276, 1994.

Alonso A, Llinás RR. Subthreshold Na^+-dependent theta-like rhythmicity in stellate cells of entorhinal cortex layer II. *Nature* 342: 175–177, 1989.

Amari S, Cichocki A, Yang H. A new learning algorithm for blind source separation. *Adv Neural Inform Process Syst* 8: 757–763, 1996.

Andersen P, Bliss TVP, Skrede KK. Lamellar organization of hippocampal excitatory pathways. *Exp Brain Res* 13: 222–238, 1971.

Anderson JS, Carandini M, Ferster D. Orientation tuning of input conductance, excitation and inhibition in cat primary visual cortex. *J Neurophysiol* 84: 909–926, 2000.

Bédard C, Kröger H, Destexhe A. Modeling extracellular field potentials and the frequency-filtering properties of extracellular space. *Biophys J* 86: 1829–1842, 2004.

Bell A, Sejnowski T. An information-maximization approach to blind separation and blind deconvolution. *Neural Comput* 7: 1129–1159, 1995.

Borg-Graham LJ, Monier C, Frégnac Y. Visual input evokes transient and strong shunting inhibition in visual cortical neurons. *Nature* 393: 369–373, 1998.

Bragin A, Jandó G, Nádasdy Z, van Landeghem M, Buzsáki G. Dentate EEG spikes and associated interneuronal population bursts in the hippocampal hilar region of the rat. *J Neurophysiol* 73: 1691–1705, 1995.

Brankačk J, Stewart M, Fox SE. Current source density analysis of the hippocampal theta rhythm: associated sustained potentials and candidate synaptic generators. *Brain Res* 615: 310–327, 1993.

Buzsáki G, Czopf J, Kondákor I, Kellényi L. Laminar distribution of hippocampal rhythmic slow activity (RSA) in the behaving rat: current-source density analysis, effects of urethane and atropine. *Brain Res* 365: 125–137, 1986.

Buzsáki G, Leung LS, Vanderwolf CH. Cellular bases of hippocampal EEG in the behaving rat. *Brain Res* 287: 139–171, 1983.

Canals S, López-Aguado L, Herreras O. Synaptically-recruited apical currents are required to initiate axonal and apical spikes in hippocampal pyramidal cells: modulation by inhibition. *J Neurophysiol* 93: 909–918, 2005.

Castellanos NP, Makarov VA. Recovering EEG brain signals: artifact suppression with wavelet enhanced independent component analysis. *J Neurosci Methods* 158: 300–312, 2006.

Choi S, Cichocki A, Park HM, Lee SY. Blind source separation and independent component analysis: a review. *Neural Inform Process Lett Rev* 6: 1–57, 2005.

Chrobak JJ, Buzsaki G. Selective activation of deep layer (V-VI) retrohippocampal cortical neurons during hippocampal sharp waves in the behaving rat. *J Neurosci* 14: 6160–6170, 1994.

Csicsvari J, Jamieson B, Wise KD, Buzsáki G. Mechanisms of gamma oscillations in the hippocampus of the behaving rat. *Neuron* 37: 311–322, 2003.

Delorme A, Makeig S. EEGLAB: an open source toolbox for analysis of single trial EEG dynamics including independent component analysis. *J Neurosci Methods* 134: 9–21, 2004.

Einevoll GT, Pettersen KH, Devor A, Ulbert I, Halgren E, Dale AM. Laminar population analysis: estimating firing rates and evoked synaptic activity from multielectrode recordings in rat barrel cortex. *J Neurophysiol* 97: 2174–2190, 2007.

Frank LM, Brown EN, Wilson MA. A comparison of the firing properties of putative excitatory and inhibitory neurons from CA1 and the entorhinal cortex. *J Neurophysiol* 86: 2029–2040, 2001.

Freeman JA, Nicholson C. Experimental optimization of current source-density technique for anuran cerebellum. *J Neurophysiol* 38: 369–382, 1975.

Hajos N, Katona I, Naiem SS, MacKie K, Ledent C, Mody I, Freund TF. Cannabinoids inhibit hippocampal GABAergic transmission and network oscillations. *Eur J Neurosci* 12: 3239–3249, 2000.

Herreras O. Propagating dendritic action potential mediates synaptic transmission in CA1 pyramidal cells in situ. *J Neurophysiol* 64: 1429–1441, 1990.

Herreras O, Solís JM, Herranz AS, Martín del Río R, Lerma J. Sensory modulation of hippocampal transmission. II. Evidence for a cholinergic locus of inhibition in the Schaffer-CA1 synapse. *Brain Res* 451: 303–313, 1988.

Herreras O, Solís JM, Martín del Río R, Lerma J. Characteristics of CA1 activation through the hippocampal trisynaptic pathway in the unanaesthetized rat. *Brain Res* 413: 75–86, 1987.

Hjorth-Simonsen A, Jeune B. Origin and termination of the hippocampal perforant path in the rat studied by silver impregnation. *J Comp Neurol* 144: 215–232, 1972.

Hyvärinen A, Oja E. Independent component analysis: algorithms and applications *Neural Netw* 13: 411–430, 2000.

Jarosiewicz B, Skaggs WE. Level of arousal during the small irregular activity state in the rat hippocampal EEG. *J Neurophysiol* 91: 2649–2657, 2004.

Jung KY, Kim JM, Kim DW, Chung CS. Independent component analysis of generalized spike-and-wave discharges: primary versus secondary bilateral synchrony. *Clin Neurophysiol* 116: 913–919, 2005.

Kandel ER, Spencer WA, Brinley FJ Jr. Electrophysiology of hippocampal neurons. I. Sequential invasion and synaptic organization. *J Neurophysiol* 24: 225–242, 1961.

Kocsis B, Bragin A, Buzsáki G. Interdependence of multiple theta generators in the hippocampus: a partial coherence analysis. *J Neurosci* 19: 6200–6212, 1999.

Lee T, Girolomi M, Sejnowski T. Independent component analysis using an extended infomax algorithm for mixed subgaussian and supergaussian sources. *Neural Comput* 11: 417–441, 1999.

Leung LS, Roth L, Canning KJ. Entorhinal inputs to hippocampal CA1 and dentate gyrus in the rat: a current-source-density study. *J Neurophysiol* 73: 2392–2403, 1995.

Lømo T. Patterns of activation in a monosynaptic cortical pathway: the perforant path input to the dentate area of the hippocampal formation. *Exp Brain Res* 12: 18–45, 1971.

López-Aguado L, Ibarz JM, Herreras O. Activity-dependent changes of tissue resistivity in the CA1 region in vivo are layer-specific: modulation of evoked potentials. *Neuroscience* 108: 249–262, 2001.

López-Aguado L, Ibarz JM, Varona P, Herreras O. Structural inhomogeneities differentially modulate action currents and population spikes initiated in the axon or dendrites. *J Neurophysiol* 88: 2809–2820, 2002.

Lorente de Nó R. Analysis of the distribution of action currents of nerves in volume conductors. In a study of nerve physiology. *Stud Rockefeller Inst Med Res Repr* 132: 384–477, 1947.

Makarov VA, Makarova J, Herreras O. Disentanglement of local field potential sources by independent component analysis. *J Comput Neurosci* In press.

Makarova J, Gómez-Galán M, Herreras O. Layer specific changes in tissue resistivity and spatial cancellation of transmembrane currents shape the voltage signal during spreading depression in the CA1 vivo. *Eur J Neurosci* 27: 444–456, 2008.

Makarova J, Makarov VA, Herreras O. A model of sustained field potentials based on gradients of polarization in single neurons. *J Neurophysiol* 103: 2446–2457, 2010.

Makeig S, Debener S, Onton J, Delorme A. Mining event-related brain dynamics. *Trends Cogn Sci* 8: 204–210, 2004.

Mann EO, Radcliffe CA, Paulsen O. Hippocampal gamma-frequency oscillations: from interneurones to pyramidal cells, and back. *J Physiol* 562: 55–63, 2005.

Miles R, Wong RK. Inhibitory control of local excitatory circuits in the guinea-pig hippocampus. *J Physiol* 388: 611–629, 1987.

Mitzdorf U. Current source-density method and application in cat cerebral cortex: investigation of evoked potentials and EEG phenomena. *Physiol Rev* 65: 37–100, 1985.

Nunez PL, Srinivasan R. *Electric Fields of the Brain: The Neurophysics of EEG* (2nd ed.). New York: Oxford, 2006.

Oren I, Hajos N, Paulsen O. Identification of the current generator underlying cholinergically induced gamma frequency field potential oscillations in the hippocampal CA3 region. *J Physiol* 588: 785–797, 2010.

Ranck JB Jr. Studies on single neurons in dorsal hippocampal formation and septum in unrestrained rats. Part 1. Behavioral correlates and firing repertoires. *Exp Neurol* 40: 462–531, 1973.

Rudolph M, Pelletier JG, Paré D, Destexhe A. Characterization of synaptic conductances and integrative properties during electrically induced EEG-activated states in neocortical neurons in vivo. *J Neurophysiol* 94: 2805–2821, 2005.

Soltesz I, Deschenes M. Low- and high-frequency membrane potential oscillations during theta activity in CA1 and CA3 pyramidal neurons of the rat hippocampus under ketamine-xylazine anesthesia. *J Neurophysiol* 70: 97–116, 1993.

Somogyi P, Klausberger T. Defined types of cortical interneurone structure space and spike timing in the hippocampus. *J Physiol* 562: 9–26, 2005.

Stone JV. *Independent Component Analysis: A Tutorial Introduction.* Cambridge, MA: MIT Press, 2004.

Tanskanen JM, Mikkonen JE, Penttonen M. Independent component analysis of neural populations from multielectrode field potential measurements. *J Neurosci Methods* 145: 213–232, 2005.

Thompson LT, Best PJ. Place cells and silent cells in the hippocampus of freely-behaving rats. *J Neurosci* 9: 2382–2390, 1989.

Varona P, Ibarz JM, López-Aguado L, Herreras O. Macroscopic and subcellular factors shaping CA1 population spikes. *J Neurophysiol* 83: 2192–2208, 2000.

Vigario R, Sarela J, Jousmaki V, Hamalainen M, Oja E. Independent component approach to the analysis of EEG and MEG recordings. *IEEE Trans Biomed Eng* 47: 589–593, 2000.

Whittington MA, Traub RD, Jefferys JGR. Synchronized oscillations in interneuron networks driven by metabotropic glutamate receptor activation. *Nature* 373: 612–615, 1995.

Wu K, Canning KJ, Leung LS. Functional interconnections between CA3 and the dentate gyrus revealed by current source density analysis. *Hippocampus* 8: 217–230, 1998.

Ylinen A, Bragin A, Nádasdy Z, Jandó G, Szabó I, Sik A, Buzsáki G. Sharp wave-associated high-frequency oscillation (200 Hz) in the intact hippocampus: network and intracellular mechanisms. *J Neurosci* 15: 30–46, 1995.